Applied Physics Letters

Measurements of a quantum bulk acoustic resonator using a superconducting qubit

Cite as: Appl. Phys. Lett. **117**, 254001 (2020); https://doi.org/10.1063/5.0023827
Submitted: 01 August 2020 • Accepted: 04 December 2020 • Published Online: 22 December 2020

M.-H. Chou, É. Dumur, Y. P. Zhong, et al.

View Online Export Citation CrossMark

ARTICLES YOU MAY BE INTERESTED IN

A quantum engineer's guide to superconducting qubits
Applied Physics Reviews **6**, 021318 (2019); https://doi.org/10.1063/1.5089550

A fast and large bandwidth superconducting variable coupler
Applied Physics Letters **117**, 244001 (2020); https://doi.org/10.1063/5.0028840

A perspective on hybrid quantum opto- and electromechanical systems
Applied Physics Letters **117**, 150503 (2020); https://doi.org/10.1063/5.0021088

Challenge us.
What are your needs for periodic signal detection?
Watch

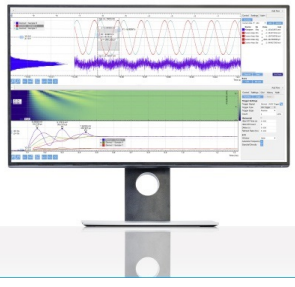

Zurich Instruments

AIP Publishing

© 2020 Author(s).

Applied Physics Letters ARTICLE scitation.org/journal/apl

Measurements of a quantum bulk acoustic resonator using a superconducting qubit

Cite as: Appl. Phys. Lett. **117**, 254001 (2020); doi: 10.1063/5.0023827
Submitted: 1 August 2020 · Accepted: 4 December 2020 ·
Published Online: 22 December 2020

View Online Export Citation CrossMark

M.-H. Chou,[1,2] É. Dumur,[1,3] Y. P. Zhong,[1] G. A. Peairs,[1,4] A. Bienfait,[1,b)] H.-S. Chang,[1] C. R. Conner,[1] J. Grebel,[1] R. G. Povey,[1,2] K. J. Satzinger,[1,4,c)] and A. N. Cleland[1,3,d)]

AFFILIATIONS

[1]Pritzker School of Molecular Engineering, University of Chicago, Chicago, Illinois 60637, USA
[2]Department of Physics, University of Chicago, Chicago, Illinois 60637, USA
[3]Argonne National Laboratory, Argonne, Illinois 60439, USA
[4]Department of Physics, University of California, Santa Barbara, California 93106, USA

[a)]**Present address:** Université Grenoble Alpes, CEA, INAC-Pheliqs, 38000 Grenoble, France.
[b)]**Present address:** Université de Lyon, ENS de Lyon, Université Claude Bernard, CNRS, Laboratoire de Physique, F-69342 Lyon, France.
[c)]**Present address:** Google, Santa Barbara CA 93117, USA.
[d)]**Author to whom correspondence should be addressed:** anc@uchicago.edu

ABSTRACT

Phonon modes at microwave frequencies can be cooled to their quantum ground state using conventional cryogenic refrigeration, providing a convenient way to study and manipulate quantum states at the single phonon level. Phonons are of particular interest because mechanical deformations can mediate interactions with a wide range of different quantum systems, including solid-state defects, superconducting qubits, and optical photons when using optomechanically active constructs. Phonons, thus, hold promise for quantum-focused applications as diverse as sensing, information processing, and communication. Here, we describe a piezoelectric quantum bulk acoustic resonator (QBAR) with a 4.88 GHz resonant frequency, which, at cryogenic temperatures, displays large electromechanical coupling strength combined with a high intrinsic mechanical quality factor, $Q_i \approx 4.3 \times 10^4$. Using a recently developed flip-chip technique, we couple this QBAR resonator to a superconducting qubit on a separate die and demonstrate the quantum control of the mechanics in the coupled system. This approach promises a facile and flexible experimental approach to quantum acoustics and hybrid quantum systems.

Published under license by AIP Publishing. https://doi.org/10.1063/5.0023827

Hybrid quantum systems have attracted significant recent interest, for applications in both quantum information processing[1–3] and quantum engineering and technology.[4–6] Quantum acoustics can play an essential role in hybrid quantum systems, as mechanical degrees of freedom can couple to many systems, including superconducting qubits,[7–15] spin ensembles,[16,17] and optical photons,[18–23] and can serve as quantum memories.[24,25] On-demand generation of single phonons has been achieved by coupling superconducting qubits via a piezoelectric interaction to film bulk acoustic resonators, to surface acoustic wave resonators, and to bulk acoustic resonators.[7,10–12,26] However, phonons do not approach the lifetimes of photons in electromagnetic cavities.[27] Here, we describe one approach that may achieve levels of performance similar to photons while affording simple lithographic fabrication.

Our quantum system comprises a high-Q electromechanical resonator made on a silicon substrate and a superconducting qubit made on a separate sapphire substrate, with both coupled using a flip-chip method.[28] This approach differs from the previous qubit-coupled experiments[7,8,13,14] where qubits were fabricated on the same substrate as the mechanical structure, yielding poor qubit performance. Here, the flip-chip approach preserves the qubit lifetime.[10–12,15,26] The mechanical resonator, shown in Fig. 1, is a mechanically suspended bilayer of single-crystal Si with a piezoelectrically active aluminum nitride (AlN) layer, actuated using an interdigital transducer (IDT), which yields a large electromechanical coupling. The structure is supported by acoustic mirrors,[24] reducing phonon leakage through the mechanical supports. The choice of materials and overall design affords more flexibility in the resonator properties, including operating frequency, mechanical mode selection, and electromechanical

Published under license by AIP Publishing

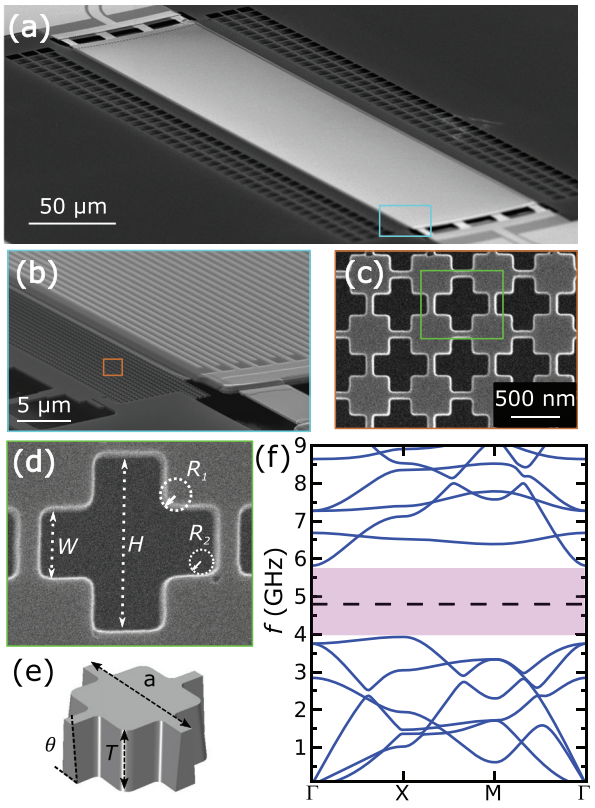

FIG. 1. Thin film quantum bulk acoustic resonator (QBAR). (a) Scanning electron micrograph (SEM) of the resonator structure, an acoustically resonant membrane $200 \times 80\ \mu m^2$ in area, made of a 220 nm thick single-crystal Si layer supporting a 330 nm thick, *c*-axis oriented piezoelectric AlN layer, supported on either side by an acoustic mirror. Actuation and detection are via an IDT comprising forty Al finger pairs, with alternate fingers connected to one of a pair of wirebond pads (not shown). (b and c) Details of the structure in (a), showing details of the IDT and the acoustic mirror supports. Each mirror is 15 phononic crystal unit cells wide, on either side of the resonator. (d) and (e) Detailed design of the phononic crystal unit cell, with dimension (H, W, R_1, R_2, *a*, *T*) = (466, 177, 40, 25, 550, 220) nm. The sidewall angle θ is ∼85°. (f) Finite-element simulation of the band structure for the phononic crystal; the dashed line indicates the QBAR resonant frequency, and the phononic crystal bandgap is shaded purple.

coupling strength, as well as allowing better mechanical isolation. The structure exhibits a resonant mechanical mode at 4.88 GHz, making the mechanical quantum ground state accessible by cooling the device to mK temperatures. We term this new design a quantum bulk acoustic resonator (QBAR).

The mechanical device is fabricated on a commercial silicon-on-insulator (SOI) wafer with a 220 nm device layer and a 2 μm buried oxide layer. We first deposit and pattern a 70 nm thick SiO_x stop layer, which protects the active device area's top Si surface from subsequent etching steps. Next, a *c*-axis oriented 330 nm thick aluminum nitride (AlN) piezoelectric layer is deposited by reactive sputter deposition,[29] using conditions that typically yield an in-plane tensile stress below 200 MPa. The AlN film is reactive-ion etched (RIE) using a reflowed photoresist mask, and the exposed underlying SiO_x stop layer is removed using buffered HF. To avoid subsequent damage to the AlN, we deposit a ∼5 nm SiO_x layer using atomic layer deposition. Phononic crystals are patterned using electron beam lithography, followed by a Cl_2/O_2 RIE. E-beam lithography defines a PMMA bilayer for liftoff of a 30 nm thick aluminum interdigital transducer (IDT) and ground plane. The wafer is diced into dies, each with closely related designs, with one die used for the classical measurements in Figs. 2 and 3 and a different die used for the quantum experiment in Fig. 4. The devices are released in HF vapor; an image is shown in Fig. 1.

The electromechanical resonator is characterized using a calibrated vector network analyzer (VNA), shown in Fig. 2. We find a strong resonant response at the electromechanical resonance frequency $f_0 = \omega_0/2\pi = 4.88$ GHz, as expected, and fit the response to a Butterworth-van Dyke model circuit (BvD),[7,30] shown in the inset in Fig. 2. This model includes the transducer electrical capacitance C_0 in parallel with the mechanical equivalent inductance and capacitance *L* and *C*, as well as a mechanical loss element *R*. The values for C_0 and *C* are determined from the known geometry and materials for the device, and the values for *L* and *R* fit to the measured response. Near the electromechanical resonance $f_0 = \sqrt{(C + C_0)/(LCC_0)}/2\pi$, the BvD model has an equivalent impedance $Z_r(f)$ given by

$$Z_r(f) \approx \frac{Q_i|Z_1|e^{i\phi}}{1 + 2iQ_i(f - f_0)/f_0}, \tag{1}$$

where $Z_1 = (1 + i\omega_0 RC - \omega_0^2 LC)/(\omega_0(C + C_0))$ with phase factor $e^{i\phi}$ and $Q_i = \sqrt{L(C + C_0)/CC_0}/R$ is the internal quality factor. The inverse transmission is

$$\tilde{S}_{21}^{-1}(f) \equiv 1 + \frac{Q_i|Z_1|e^{i\phi}}{2Z_0}\frac{1}{1 + i2Q_i(f - f_0)/f_0}, \tag{2}$$

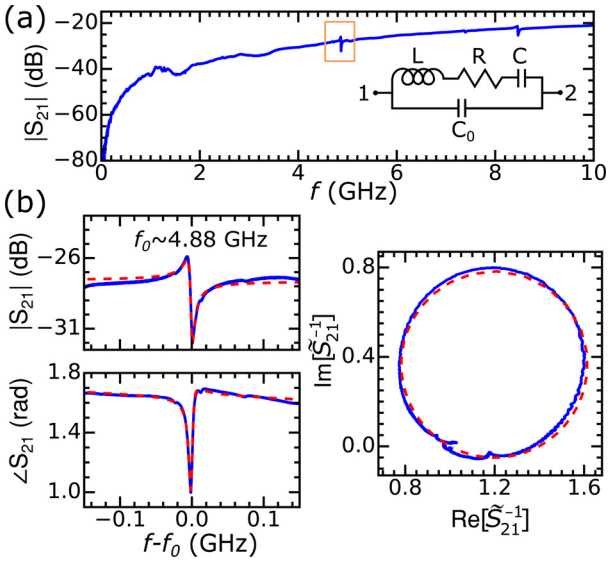

FIG. 2. Room temperature microwave transmission measurements. (a) Main panel shows the transmission magnitude $|S_{21}|$ measured by a vector network analyzer (VNA) connected via a microwave probe station. The inset shows the equivalent electrical circuit, based on the Butterworth-van Dyke model; 1 and 2 correspond to VNA ports. (b) Left: Magnitude $|S_{21}|$ and phase $\angle S_{21}$ (blue) near the QBAR electromechanical resonance at $f_0 = 4.88$ GHz. Right: Inverse $1/\tilde{S}_{21}$ (blue) in the complex plane (horizontal axis: real part; vertical axis: imaginary part). Dashed lines (red) are fits to Eq. (2).

Published under license by AIP Publishing

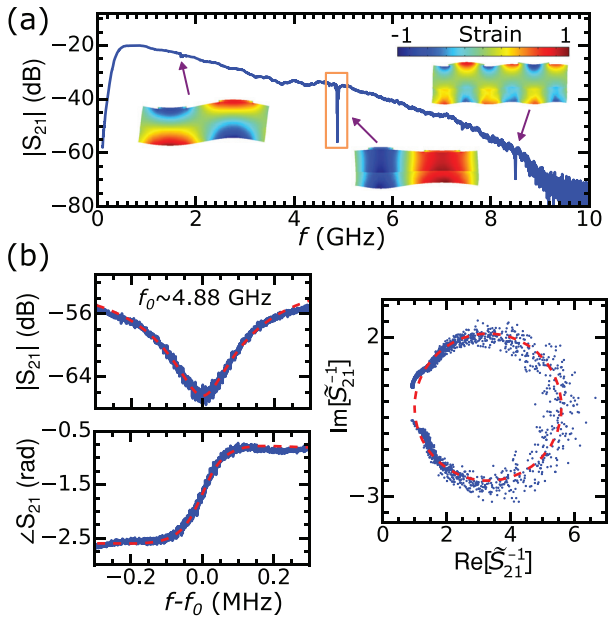

FIG. 3. Microwave transmission measurements at $T \sim 80$ mK. (a) Transmission magnitude $|S_{21}|$ displays three resonances at 1.69, 4.88, and 8.50 GHz, in reasonable agreement with simulations, shown as strain maps (normalized) (inset). (b) Left: Details of the primary resonance at $f_0 = 4.88$ GHz, plotted in amplitude and phase vs detuning $f - f_0$. Right: $\tilde{S}_{21}^{-1}$ plotted in the complex plane (blue). Dashed lines (red) are fits to Eq. (2). We estimate the excitation corresponding to $\sim 10^6$ phonons.

where $Z_0 = 50\,\Omega$. A fit to the data (Fig. 2) yields the internal quality factor $Q_i \sim 1.0 \times 10^3$ (measured at room temperature).

We characterize the resonator at temperatures below 1 K using an adiabatic demagnetization refrigerator (base temperature, ~60 mK). Excitation signals from a VNA with −40 dBm output power, which corresponds to about 10^6 phonons in the cavity, pass through a 20 dB attenuator, with the reflection from the device amplified by room-temperature amplifiers with a net gain of 20 dB. The results are displayed in Fig. 3. The resonant frequency remains unchanged from room temperature, while Q_i increases by a factor of 40 to $Q_i \sim 4.3 \times 10^4$. As substrate loss is significantly decreased at cryogenic temperatures, additional resonant modes become detectable, consistent with finite-element simulations, shown in Fig. 3(a).

A superconducting qubit is a unique tool to characterize mechanical resonators in the quantum limit.[7,10–15,26] Here, we use a frequency-tunable planar Xmon qubit[31,32] to characterize a QBAR very similar to that measured classically. The qubit is fabricated on a separate sapphire die, with wiring on the two dies including mutual inductive couplers;[28] a schematic is shown in Fig. 4a. The sapphire and SOI dies are aligned and attached to one another using photoresist, with vertical spacing defined by ~5 μm thick spacers.[28] A flux-tunable coupler element[10] is placed between the qubit and its mutual coupling inductance, allowing the external flux control of the coupling strength, from zero to a maximum of $2g/2\pi \sim 11.2$ MHz.

With the coupler off (coupling rate, $2g/2\pi \approx 0$ MHz), we measure the intrinsic qubit $T_1^{qb} = 10\,\mu$s and $T_{2,Ramsey}^{qb} = 1\,\mu$s, for qubit frequencies ranging from 4.5 to 5.0 GHz, with both measured using

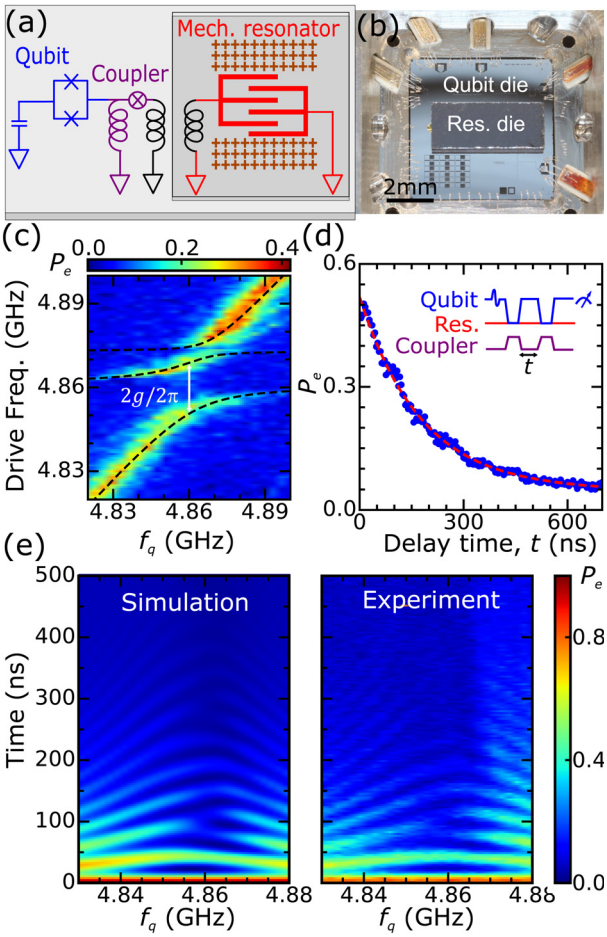

FIG. 4. Qubit-mediated measurements of the mechanical resonator. (a) Electrical circuit diagram, showing qubit (blue) and tunable coupler (purple), one arm of which couples inductively (black) to the IDT (red). Two acoustic mirrors consist of phononic crystal arrays (brown). (b) Photograph of flip-chip assembly, comprising a 6×6 cm^2 qubit die (bottom) and a 4×2 cm^2 resonator die (top). (c) Qubit spectroscopy, showing excited state probability P_e vs qubit frequency (horizontal) and microwave pulse frequency (vertical). An avoided-level crossing appears when the qubit and resonator are in resonance. Two energy splittings can be observed, with the larger corresponding to the primary mechanical mode ($2g/2\pi \sim 9.6$ MHz) and the other a spurious mechanical mode ($2g_{spur}/2\pi \sim 3.5$ MHz). Dashed lines (black) are fits to a modified Jaynes–Cummings model including two resonant modes. (d) Phonon lifetime measurement. The inset shows the pulse sequence. The main panel shows the qubit final excited state probability P_e, where the exponential decay is primarily due to the phonon lifetime of 178 ns, as fit by the dashed line (red). (e) Qubit-resonator Rabi swaps. The probability of the qubit excited state P_e (color scale) is plotted vs qubit frequency f_q (horizontal) and qubit-resonator interaction time (vertical). Coupling strengths are $2g/2\pi \sim 11.2$ MHz and $2g_{spur}/2\pi \sim 3.5$ MHz for primary and spurious mechanical modes, respectively. Left: simulation results. Right: experimental results.

standard techniques.[32] As we increase the coupling strength from zero, the qubit response includes the resonator and becomes more complex, in particular near the resonator frequency. In Fig. 4(c), we show a qubit spectroscopy measurement with the coupler set to a coupling $2g/2\pi = 9.6$ MHz. After setting the qubit frequency (horizontal axis),

Published under license by AIP Publishing

the qubit is gently excited by a 1 μs excitation microwave tone at the drive frequency (vertical axis) and the qubit excited state probability P_e measured (color scale). The qubit tunes as expected, exhibiting the expected splitting as it crosses the mechanical resonator frequency at $f_r = 4.86$ GHz. There is an additional spurious mode that is weakly coupled to the qubit at 4.87 GHz, with a splitting of about $2g_{spur}/2\pi = 3.5$ MHz. This spurious mode may come from a slight difference between the IDT resonant frequency and that of the QBAR.

We next use the qubit to perform a single-phonon lifetime measurement,[7] using the pulse sequence in Fig. 4(d). From the decay of $P_e(t)$ with delay t, we extract the resonator's energy relaxation time $T_{1,r} = 178 \pm 2$ ns. This corresponds to a single-phonon quality factor $Q_i \sim (5.43 \pm 0.06) \times 10^3$, slightly smaller than the device measured in Fig. 3. We believe that the reduction in the quality factor compared to the measurements shown in Fig. 3 is due to spurious two-level system defects[33,34] that are saturated at the higher powers ($\sim 10^6$ phonons) used in Fig. 3 compared to the single-phonon energies used here.[35]

In Fig. 4(e), we display a qubit-resonator Rabi swap, measured as a function of time (vertical axis) and as a function of qubit detuning from the resonator frequency (horizontal axis). A microwave pulse places the qubit in its excited state, and the coupling between the qubit and resonator is turned on, initiating the Rabi swap. By measuring the qubit state at different times, we capture the excitation as it is exchanged between the qubit and resonator, whereas the qubit-resonator detuning increases, the swap rate increases, but the amplitude decreases. The spurious mode interferes with this process, generating a non-ideal response, consistent with the spectroscopy measurement. The lifetime of the Rabi swap process is significantly shorter than that measured in Fig. 4(d), implying that an unknown additional loss is introduced when we leave the qubit variable coupler on.

We used numerical simulations to support our experimental results. The simulations use a modified Jaynes–Cummings model, where the qubit is modeled as a two-level system coupled to two harmonic oscillators, representing the main and spurious mechanical modes, with different coupling strengths at the frequencies 4.86 and 4.87 GHz, respectively. Both the avoided-level crossing in Fig. 4(c) and the Rabi swap measurement in Fig. 4(e) are supported by this model, from which we extract a $T_{1,r}^{spur}$ lifetime for the spurious mode of ~ 70 ns.

In conclusion, we have designed and fabricated a microwave-frequency quantum bulk acoustic resonator with a resonance frequency just below 5 GHz and a single-phonon intrinsic quality factor of $Q_i \sim (5.43 \pm 0.06) \times 10^3$; a companion device measured with a VNA has $Q_i \sim 4.3 \times 10^4$. These quality factors are roughly 20 times and 200 times higher than those obtained in our previous experiment on thin-film bulk acoustic resonators,[7] although they do not yet approach those on wafer-thickness bulk resonators.[9,11,36,37] The piezoelectric construction of the resonator supports a strong electromechanical coupling rate, allowing us to couple it to a superconducting qubit for quantum measurements. This approach holds promise for high quality factor, very small form-factor resonant acoustic cavities operating in the quantum limit, with potential applications to hybrid quantum systems, quantum communication, and quantum computing.

The authors thank P. J. Duda for fabrication assistance and F. J. Heremans and N. Delegan for help with the AlN sputter system. Devices and experiments were supported by the Air Force Office of Scientific Research and the Army Research Laboratory. K.J.S. was supported by NSF GRFP (NSF No. DGE-1144085), É.D. was supported by LDRD funds from Argonne National Laboratory, and A.N.C. was supported in part by the DOE, Office of Basic Energy Sciences. This work was partially supported by the UChicago MRSEC (NSF No. DMR-1420709) and made use of the Pritzker Nanofabrication Facility, which receives support from SHyNE, a node of the National Science Foundation's National Nanotechnology Coordinated Infrastructure (No. NSF NNCI-1542205).

The authors declare no competing financial interest.

DATA AVAILABILITY

The data that support the findings of this study are available from the corresponding author upon reasonable request.

REFERENCES

[1] Z.-L. Xiang, S. Ashhab, J. Q. You, and F. Nori, Rev. Mod. Phys. **85**, 623 (2013).
[2] M. Aspelmeyer, T. J. Kippenberg, and F. Marquardt, Rev. Mod. Phys. **86**, 1391 (2014).
[3] A. A. Clerk, K. W. Lehnert, P. Bertet, J. R. Petta, and Y. Nakamura, Nat. Phys. **16**, 257 (2020).
[4] G. Kurizki, P. Bertet, Y. Kubo, K. Mølmer, D. Petrosyan, P. Rabl, and J. Schmiedmayer, Proc. Natl. Acad. Sci. U. S. A. **112**, 3866 (2015).
[5] C. L. Degen, F. Reinhard, and P. Cappellaro, Rev. Mod. Phys. **89**, 035002 (2017).
[6] J. J. Morton and P. Bertet, J. Magn. Reson. **287**, 128 (2018).
[7] A. D. O'Connell, M. Hofheinz, M. Ansmann, R. C. Bialczak, M. Lenander, E. Lucero, M. Neeley, D. Sank, H. Wang, M. Weides, J. Wenner, J. M. Martinis, and A. N. Cleland, Nature **464**, 697 (2010).
[8] M. V. Gustafsson, T. Aref, A. F. Kockum, M. K. Ekstrom, G. Johansson, and P. Delsing, Science **346**, 207 (2014).
[9] Y. Chu, P. Kharel, W. H. Renninger, L. D. Burkhart, L. Frunzio, P. T. Rakich, and R. J. Schoelkopf, Science **358**, 199 (2017).
[10] K. J. Satzinger, Y. P. Zhong, H.-S. Chang, G. A. Peairs, A. Bienfait, M.-H. Chou, A. Y. Cleland, C. R. Conner, É. Dumur, J. Grebel, I. Gutierrez, B. H. November, R. G. Povey, S. J. Whiteley, D. D. Awschalom, D. I. Schuster, and A. N. Cleland, Nature **563**, 661 (2018).
[11] Y. Chu, P. Kharel, T. Yoon, L. Frunzio, P. T. Rakich, and R. J. Schoelkopf, Nature **563**, 666 (2018).
[12] A. Bienfait, K. J. Satzinger, Y. P. Zhong, H.-S. Chang, M.-H. Chou, C. R. Conner, É. Dumur, J. Grebel, G. A. Peairs, R. G. Povey, and A. N. Cleland, Science **364**, 368 (2019).
[13] P. Arrangoiz-Arriola, E. A. Wollack, Z. Wang, M. Pechal, W. Jiang, T. P. McKenna, J. D. Witmer, R. Van Laer, and A. H. Safavi-Naeini, Nature **571**, 537 (2019).
[14] L. R. Sletten, B. A. Moores, J. J. Viennot, and K. W. Lehnert, Phys. Rev. X **9**, 021056 (2019).
[15] M. Kervinen, A. Välimaa, J. E. Ramírez-Muñoz, and M. A. Sillanpää, Phys. Rev. Appl. **14**, 054023 (2020).
[16] S. J. Whiteley, G. Wolfowicz, C. P. Anderson, A. Bourassa, H. Ma, M. Ye, G. Koolstra, K. J. Satzinger, M. V. Holt, F. J. Heremans, A. N. Cleland, D. I. Schuster, G. Galli, and D. D. Awschalom, Nat. Phys. **15**, 490 (2019).
[17] H. Chen, N. F. Opondo, B. Jiang, E. R. MacQuarrie, R. S. Daveau, S. A. Bhave, and G. D. Fuchs, Nano Lett. **19**, 7021 (2019).
[18] J. Chan, T. M. Alegre, A. H. Safavi-Naeini, J. T. Hill, A. Krause, S. Gröblacher, M. Aspelmeyer, and O. Painter, Nature **478**, 89 (2011).
[19] A. H. Safavi-Naeini, J. Chan, J. T. Hill, T. P. M. Alegre, A. Krause, and O. Painter, Phys. Rev. Lett. **108**, 033602 (2012).
[20] J. Bochmann, A. Vainsencher, D. D. Awschalom, and A. N. Cleland, Nat. Phys. **9**, 712 (2013).
[21] A. Vainsencher, K. Satzinger, G. Peairs, and A. Cleland, Appl. Phys. Lett. **109**, 033107 (2016).

Published under license by AIP Publishing

[22]S. Hong, R. Riedinger, I. Marinković, A. Wallucks, S. G. Hofer, R. A. Norte, M. Aspelmeyer, and S. Gröblacher, Science **358**, 203 (2017).
[23]R. Riedinger, A. Wallucks, I. Marinković, C. Löschnauer, M. Aspelmeyer, S. Hong, and S. Gröblacher, Nature **556**, 473 (2018).
[24]G. S. MacCabe, H. Ren, J. Luo, J. D. Cohen, H. Zhou, A. Sipahigil, M. Mirhosseini, and O. Painter, Science **370**, 840 (2020).
[25]H. Ren, M. H. Matheny, G. S. MacCabe, J. Luo, H. Pfeifer, M. Mirhosseini, and O. Painter, Nat. Commun. **11**, 3373 (2020).
[26]A. Bienfait, Y. P. Zhong, H.-S. Chang, M.-H. Chou, C. R. Conner, É. Dumur, J. Grebel, G. A. Peairs, R. G. Povey, K. J. Satzinger, and A. N. Cleland, Phys. Rev. X **10**, 021055 (2020).
[27]A. Romanenko, R. Pilipenko, S. Zorzetti, D. Frolov, M. Awida, S. Belomestnykh, S. Posen, and A. Grassellino, Phys. Rev. Appl. **13**, 034032 (2020).
[28]K. J. Satzinger, C. R. Conner, A. Bienfait, H.-S. Chang, M.-H. Chou, A. Y. Cleland, É. Dumur, J. Grebel, G. A. Peairs, R. G. Povey, S. J. Whiteley, Y. P. Zhong, D. D. Awschalom, D. I. Schuster, and A. N. Cleland, Appl. Phys. Lett. **114**, 173501 (2019).
[29]V. Felmetsger, P. Laptev, and S. Tanner, J. Vac. Sci. Technol., A **27**, 417 (2009).
[30]J. D. Larson, J. Ruby, R. Bradley, J. Wen, S.-L. Kok, and A. Chien, in *IEEE Ultrasonics Symposium. Proceedings. An International Symposium* (IEEE, 2000),Vol. 1, pp. 869–874.
[31]J. Koch, T. M. Yu, J. Gambetta, A. A. Houck, D. I. Schuster, J. Majer, A. Blais, M. H. Devoret, S. M. Girvin, and R. J. Schoelkopf, Phys. Rev. A **76**, 042319 (2007).
[32]R. Barends, J. Kelly, A. Megrant, D. Sank, E. Jeffrey, Y. Chen, Y. Yin, B. Chiaro, J. Mutus, C. Neill, P. O'Malley, P. Roushan, J. Wenner, T. C. White, A. N. Cleland, and J. M. Martinis, Phys. Rev. Lett. **111**, 080502 (2013).
[33]G. Andersson, A. L. O. Bilobran, M. Scigliuzzo, M. M. de Lima, J. H. Cole, and P. Delsing, arXiv:2002.09389 (2020).
[34]E. A. Wollack, A. Y. Cleland, P. Arrangoiz-Arriola, T. P. McKenna, R. G. Gruenke, R. N. Patel, W. Jiang, C. J. Sarabalis, and A. H. Safavi-Naeini, arXiv:2010.01025 (2020).
[35]A. Megrant, C. Neill, R. Barends, B. Chiaro, Y. Chen, L. Feigl, J. Kelly, E. Lucero, M. Mariantoni, P. J. O'Malley *et al.*, Appl. Phys. Lett. **100**, 113510 (2012).
[36]W. Renninger, P. Kharel, R. Behunin, and P. Rakich, Nat. Phys. **14**, 601 (2018).
[37]V. J. Gokhale, B. P. Downey, D. S. Katzer, N. Nepal, A. C. Lang, R. M. Stroud, and D. J. Meyer, Nat. Commun. **11**(1), 2314 (2020).

Published under license by AIP Publishing